Modeling the crystal-field splitting of the energy levels of Er^{3+} in charge-compensated sites in lithium niobate

John B. Gruber
Department of Physics, San José State University, San Jose, California 95192-0106, USA

Dhiraj K. Sardar and Raylon M. Yow
Department of Physics and Astronomy, University of Texas at San Antonio, San Antonio, Texas 78249-0663, USA

Bahram Zandi
ARL/Adelphi Laboratory Center, 2800 Powder Mill Road, Adelphi, Maryland 20783-1197, USA

Edvard P. Kokanyan
Institute for Physical Research, National Academy of Sciences of Armenia, 378410, Ashtarak-2, Armenia
(Received 17 December 2003; published 6 May 2004)

We have calculated the crystal-field splitting of the energy levels of $Er^{3+}(4f^{11})$ in charge-compensated sites having C_3 symmetry in the host crystal of lithium niobate, $LiNbO_3$ (LN), with crystal-field parameters obtained from lattice-sum calculations. The charge-compensation model assumes that Er^{3+} substitutes into Li^+ sites that are shifted from the Li^+ positions in the undoped lattice with excess charge compensated for by niobium vacancies and defect complexes. The calculated splitting of 11 multiplet manifolds $^{2S+1}L_J$ including the ground state $^4I_{15/2}$ of $Er^{3+}(4f^{11})$ is compared with existing data in the literature, as well as with polarized absorption and fluorescence spectra obtained in the present study between 8 K and room temperature. The calculated splitting is compared with the experimental splitting without least-squares adjustments to the crystal-field splitting parameters, although the centroids between multiplet manifolds are adjusted to account for J mixing between states. The calculated splitting supports site symmetries for Er^{3+} as C_3, in agreement with magnetic resonance studies. The calculation also predicts the symmetry label of the ground-state Stark level as $^2\Gamma_6$ or $\mu(\pm 3/2)$, in agreement with the observed polarized absorption and fluorescence spectra.

DOI: 10.1103/PhysRevB.69.195103 PACS number(s): 42.70.Hj, 78.40.−q, 71.70.Ch

I. INTRODUCTION

Crystals of $LiNbO_3$ (LN) are piezoelectric, pyroelectric, and optically nonlinear, which makes them components of choice for many integrated electro-optical circuits and devices.[1–12] Unfortunately, these crystals are also highly susceptible to optical damage that brings about light-induced refractive index changes, which further limit possible applications.[13–17] As part of our studies on reducing photorefraction in LN crystals, we have recently grown periodically poled, as well as single-domain LN crystals containing Hf^{4+} and Zr^{4+} by the Czochralski method.[18] We have also grown single-domain LN crystals of high optical quality containing Er^{3+} with Er_2O_3 as a dopant in the melt.[19] The spectroscopic properties of these crystals have been investigated because of their importance in the design of waveguide lasers in the infrared and waveguide amplifiers.[13,20–23] Crystals in which photorefraction is reduced by adding HfO_2 and ZrO_2 to the melt offer further possibilities for adapting the observed Er^{3+} upconversion phenomena for telecommunication purposes.[20–26]

In the present study, we report the synthesis and growth of Er^{3+}:LN crystals and the spectroscopic properties of these crystals in light of the existing literature on samples grown by different means and with different dopants used to reduce photorefraction. Recent results on the detailed crystal structure[27–31] and site-selective spectroscopy on Er^{3+}:LN (Refs. 25, 32, and 33) have encouraged us to carry out a detailed lattice-sum calculation for crystal-field parameters, useful in establishing the crystal-field splitting of the energy levels of Er^{3+} ions in charge-compensated sites in the LN lattice.[34–36] To support these calculations, we present the polarized absorption spectra obtained between 400 and 1600 nm and fluorescence spectra between 540 and 580 nm and between 1500 and 1650 nm at temperatures between 8 K and room temperature. A total of 11 multiplet manifolds $^{2S+1}L_J$ of $Er^{3+}(4f^{11})$ in LN is analyzed and compared with crystal-field splitting calculations.

II. CRYSTAL GROWTH AND STRUCTURE

High-purity compounds from Johnson-Mattey (Nb_2O_5) and Merck (Li_2CO_3) in powder form were used as the starting materials for preparing the LN charges. The Er^{3+} concentration was approximately 1 wt % when added to the initial melt in the form of Er_2O_3 (99.99%, Merck). Crystals of Er^{3+}:LN having a congruent composition were grown by the Czochralski method in air using a setup with a platinum crucible that had dimensions of 50 mm×3 mm×50 mm. The crucible was heated in a rf furnace. The ferroelectric critical temperature of the congruent (Li/Nb=0.946) composition crystal is about 1142 °C, just 110° below the melting point of 1253 °C. To obtain single-domain crystals containing Er^{3+} directly during the growth process, we applied an electric field (a dc electrical current of 12 A/m^2) to the

crystal-melt system.[19] Without the application of an external electric field, the crystals grow in the paraelectric phase. Multidomains then appear as the sample is cooled below the Curie temperature, and an additional post-growth annealing procedure is required. The application of an electric field to the crystal-melt system during crystal growth leads to a homogeneous distribution of impurity ions within the main constituents that form the crystal.[19] Crystals were pulled along the *c* axis at the rate of 1 mm/h and at a rotation speed of 20 rpm. Further details are provided in an earlier publication.[18,37] To determine the amount of Er in the crystals that were grown, we had a crystal analyzed for Er by Galbraith Laboratories, Knoxville, TN. They reported 0.88 wt % Er. According to Bermudez *et al.*,[38] the distribution coefficient for Er in congruent LN is approximately 1, consistent with our expectations in the present study and the error associated with the analysis for Er.

The single-domain crystals used in the present study were of high optical quality. Many of the measured photorefractive properties of these crystals have been reported by some of us earlier as a function of Hf^{4+} and Zr^{4+} concentrations.[18,37] For the spectroscopic studies of Er^{3+} reported here, single-crystal boules having dimensions of 20 mm in diameter and 30 mm in length were oriented by Laue x-ray diffraction and cut perpendicularly to the *b* axis (*Y* cut). From these boules, crystal plates (10 mm$\times$3 mm$\times$10 mm) were cut and polished along the *Y* plane.

The crystal structure of congruent lithium niobate (LN) is described by the space group $C_{3v}^{6}(R3c)$, where Li^{+} occupies the [0,0,1/4] position and Nb^{5+} occupies the [0,0,0] position, both on the trigonal axis.[28,29] Dopant ions such as Er^{3+} occupy charge-compensated sites near these cationic sites[27,39] or in an interstitial position also associated with the *c* axis [0,0,1/6].[40–42] From electron spin resonance (ESR) studies, the point-group symmetry of the Er^{3+} ions in LN is reported as C_3.[39,43,44] By using x-ray standing waves, Gog *et al.*[27] were able to identify the Er in Li sites, but the ions were shifted from the undoped Li position along the direction of the *c* axis, still having C_3 point-group symmetry. Using ion-beam channeling techniques, Rebouta *et al.*[40–42] concluded that Er lies at the Li octahedron with a shift of about 0.2 Å from the regular Li site. Drawings of the crystal structure and relationship of the Er^{3+} ions to the site symmetry (C_3) are found in these publications.[27,39,40–43] For our calculations, we have made use of the drawings in Figs. 3 and 4 of Ref. 27 since this work also describes the specific mechanism which we used in our investigations.

III. EXPERIMENTAL INSTRUMENTATION

Absorption spectra were obtained from an upgraded Cary Model 14R spectrophotometer controlled by a desktop computer. The spectral bandwidth was set at 0.1 nm for all measurements, and the instrument was calibrated internally to better than 0.3 nm. Fluorescence spectra were collected at right angles with respect to the direction of the excitation source and focused on the entrance slit of a SPEX model 340E scanning monochromator. Spectral resolution was better than 0.1 nm for all wavelengths investigated, and the wavelength reproducibility of the monochromator was better than 0.01 nm. A desktop computer was used to control the monochromator and to acquire and analyze the fluorescence data.

The excitation source for the fluorescence studies was the 514.5-nm emission peak from an argon-ion laser, Spectra Physics model 2005. A photomultiplier tube was used to detect fluorescence between 540 and 580 nm ($^4S_{3/2}\rightarrow{}^4I_{15/2}$) and a Ge diode cooled with liquid nitrogen was used to detect fluorescence between 1500 and 1650 nm ($^4I_{13/2}\rightarrow{}^4I_{15/2}$). Polarized absorption and emission spectra were obtained by using cross polaroids or a Glan-Thompson calcite polarizer.

Spectra were obtained at temperatures between 8 K and room temperature by mounting the sample on a copper block on the cold finger of a closed-cycle helium cryogenic refrigerator, CTI model 22. The sample temperature was monitored with a silicon-diode sensor attached to the base of the sample holder and maintained at a programmed temperature by a Lake Shore temperature control unit. Since the sample is cooled by conduction and the sensor is not placed directly on the sample, we suspect the actual temperature is somewhat higher. For that reason we quote a nominal temperature in the text.

IV. ABSORPTION SPECTRA

Table I lists the absorption spectrum for ten excited multiplet manifolds $^{2S+1}L_J$ of Er^{3+}:LN observed between 400 and 1600 nm and obtained at a nominal temperature of 8 K. Intensities of the unpolarized spectrum appear in column 3 with Fig. 1 (the $^4I_{13/2}$ manifold) as an example of the unpolarized spectra obtained at 8, 80, and 200 K. Spectra were also obtained with light polarized parallel and perpendicular to the optical axis (the *c* axis) of the crystal. Examples of polarized spectra are shown in Fig. 2 (the $^4I_{9/2}$ manifold), Fig. 3 (the $^4S_{3/2}$ and $^2H_{11/2}$ manifolds), and Fig. 4 (the $^4F_{7/2}$, $^4F_{5/2}$, and $^4F_{3/2}$ manifolds). The polarization assignments given in Table I for the $^2H_{11/2}$, $^4S_{3/2}$, and $^4F_{9/2}$ (Column 4) are in agreement with those reported by Witte *et al.*[25] Absorption peaks that are partially polarized with the absorption stronger in one polarization relative to the other are assigned according to the stronger polarization and are marked with an asterisk in column 4, Table I. Polarization data are valuable in making Stark-level symmetry label assignments. The absorption spectrum appearing in Table I represents transitions (column 5) from the ground-state Stark level Z_1 in the $^4I_{15/2}$ multiplet manifold to Stark levels in excited $^{2S+1}L_J$ manifolds.

Absorption by individual excited multiplet manifolds at 8 K usually consists of more than the expected $J+\frac{1}{2}$ absorption peaks for Er^{3+} ions in a single site. In some cases, several relatively sharp peaks are clustered about a stronger peak, and in other cases, the peaks are relatively broad, showing evidence of unresolved structure. For example, in Fig. 2 (the $^4I_{9/2}$ manifold) we observe clusters of absorption peaks around 793, 797, and 806 nm. The spectrum of the $^4S_{3/2}$ manifold (Fig. 3) is characterized by two absorption bands with shoulders. The most clearly resolved structure is

TABLE I. Absorption spectrum of Er^{3+} in $LiNbO_3$ (8 K).

$^{2S+1}L_J$[a]	λ (nm)[b]	α (cm^{-1})[c]	Pol.[d]	Trans.[e]	E (cm^{-1})[f] obs.	E (cm^{-1})[g] calc.	μ[h]	Percent free-ion state
$^4I_{13/2}$	1532.2(sh)	3.81			6525			
(6682)	1531.3	6.67	σ*	$Z_1 \rightarrow Y_1$	6529	6529	$\pm 1/2$	$99.9\,^4I_{13/2} + 0.03\,^4I_{11/2} + 0.02\,^4I_{15/2}$
	1530(sh)	1.23			6534			
	1517.2	0.88			6589			
	1513.0	0.89	σ	$Z_1 \rightarrow Y_2$	6608	6610	$\pm 1/2$	$99.9\,^4I_{13/2} + 0.05\,^4I_{11/2} + 0.01\,^4I_{15/2}$
	1510.2	0.96			6620			
	1508.4	0.85			6628			
	1506.8	0.74	π*	$Z_1 \rightarrow Y_3$	6635	6639	$\pm 3/2$	$99.8\,^4I_{13/2} + 0.08\,^4I_{11/2} + 0.03\,^4I_{15/2}$
	1504.9	0.73	σ	$Z_1 \rightarrow Y_4$	6645	6654	$\pm 1/2$	$99.8\,^4I_{13/2} + 0.09\,^4I_{11/2} + 0.02\,^4I_{15/2}$
	1485(sh)	0.97	—	$Z_1 \rightarrow Y_5$	6732	6730	$\pm 1/2$	$99.8\,^4I_{13/2} + 0.05\,^4I_{11/2} + 0.05\,^4I_{15/2}$
	1478.0	2.11			6764			
	1475.4	2.02	π*	$Z_1 \rightarrow Y_6$	6776	6772	$\pm 3/2$	$99.8\,^4I_{13/2} + 0.11\,^4I_{11/2} + 0.03\,^4I_{15/2}$
	1471.5	1.10			6794			
	1469.2	1.08	σ	$Z_1 \rightarrow Y_7$	6805	6805	$\pm 1/2$	$99.9\,^4I_{13/2} + 0.09\,^4I_{11/2} + 0.01\,^4G_{9/2}$
$^4I_{11/2}$	980.6	1.26			10195			
(10301)	980.1	1.46	σ		10200			
	979.6	1.52		$Z_1 \rightarrow X_1$	10205	10204	$\pm 1/2$	$99.8\,^4I_{11/2} + 0.07\,^4I_{13/2} + 0.03\,^4F_{9/2}$
	974.9	1.46			10255			
	974.4	1.57	π*	$Z_1 \rightarrow X_2$	10260	10262	$\pm 3/2$	$99.8\,^4I_{11/2} + 0.07\,^4I_{9/2} + 0.04\,^4I_{13/2}$
	972(sh)	1.25		$Z_1 \rightarrow X_3$	10280	10286	$\pm 1/2$	$99.8\,^4I_{11/2} + 0.05\,^4I_{13/2} + 0.04\,^4I_{9/2}$
	969.0	1.40	σ	$Z_1 \rightarrow X_4$	10317	10326	$\pm 1/2$	$99.8\,^4I_{11/2} + 0.14\,^4I_{13/2} + 0.04\,^4F_{9/2}$
	967(sh)	0.40	—	$Z_1 \rightarrow X_5$	10340	10343	$\pm 3/2$	$99.7\,^4I_{11/2} + 0.15\,^4I_{13/2} + 0.09\,^4F_{9/2}$
	965(sh)	0.20	—	$Z_1 \rightarrow X_6$	10360	10366	$\pm 1/2$	$99.8\,^4I_{11/2} + 0.10\,^4I_{9/2} + 0.05\,^4I_{13/2}$
$^4I_{9/2}$	808.2	1.34	σ		12370			
(12491)	807.8	1.89	π	$Z_1 \rightarrow W_1$	12376	12381	$\pm 3/2$	$99.9\,^4I_{9/2} + 0.06\,^4I_{11/2} + 0.02\,^4F_{9/2}$
	807.0	1.31	σ		12388			
	805.9	1.25	σ	$Z_1 \rightarrow W_2$	12405	12407	$\pm 1/2$	$99.8\,^4I_{9/2} + 0.11\,^4F_{11/2} + 0.05\,^4I_{11/2}$
	805.6	1.22	π		12410			
	801(b)	—	—	$Z_1 \rightarrow W_3$	12480	12485	$\pm 1/2$	$99.8\,^4I_{9/2} + 0.08\,^4I_{11/2} + 0.02\,^2H_{11/2}$
	797.6	1.35			12534			
	797.4	1.32			12537			
	797.1	1.35	π	$Z_1 \rightarrow W_4$	12542	12540	$\pm 3/2$	$99.8\,^4I_{9/2} + 0.08\,^4I_{11/2} + 0.07\,^4F_{9/2}$
	796.2	1.38			12556			
	793.8	1.07			12597			
	793.3	1.04	σ	$Z_1 \rightarrow W_5$	12610	12619	$\pm 1/2$	$99.9\,^4I_{9/2} + 0.06\,^4F_{9/2} + 0.03\,^2H_{11/2}$
	793.1	1.07			12612			
$^4F_{9/2}$	659.8	1.70	σ	$Z_1 \rightarrow V_1$	15152	15151	$\pm 1/2$	$99.9\,^4F_{9/2} + 0.05\,^4I_{9/2} + 0.04\,^4F_{5/2}$
(15253)	658.3	1.06			15186			
	658.1	1.14	π	$Z_1 \rightarrow V_2$	15191	15177	$\pm 3/2$	$99.8\,^4F_{9/2} + 0.05\,^4I_{9/2} + 0.04\,^4I_{11/2}$
	657.9	1.27			15196			
	655.7	1.08			15247			
	655.2	1.37	σ	$Z_1 \rightarrow V_3$	15258	15255	$\pm 1/2$	$99.8\,^4F_{9/2} + 0.08\,^2H_{11/2} + 0.07\,^4I_{11/2}$
	655(sh)	1.11			15263			
	652.1	1.49	σ		15331	15318	$\pm 1/2$	$99.8\,^4F_{9/2} + 0.13\,^2H_{11/2} + 0.03\,^4I_{11/2}$
	651.8	1.73		$Z_1 \rightarrow V_4$	15338			
	651.4	2.20	π	$Z_1 \rightarrow V_5$	15347	15349	$\pm 3/2$	$99.6\,^4F_{9/2} + 0.17\,^2H_{11/2} + 0.12\,^4I_{9/2}$
	650.6	1.41			15366			
$^4S_{3/2}$	547.6	0.86	σ	$Z_1 \rightarrow U_1$	18256	18254	$\pm 1/2$	$97.8\,^4S_{3/2} + 2.14\,^2H_{11/2} + 0.02\,^4I_{9/2}$
(18327)	547(sh)	0.84			18260			

TABLE I. (*Continued*.)

$^{2S+1}L_J$[a]	λ (nm)[b]	α (cm^{-1})[c]	Pol.[d]	Trans.[e]	E (cm^{-1})[f] obs.	E (cm^{-1})[g] calc.	μ[h]	Percent free-ion state
	545(sh)	1.30			18344			
	544.7	1.09	π	$Z_1 \rightarrow U_2$	18354	18361	$\pm 3/2$	$97.3^4S_{3/2}+2.60^2H_{11/2}+0.05^4I_{9/2}$
$^2H_{11/2}$	526.4	2.83			18992			
(19070)	526.0	3.07	σ	$Z_1 \rightarrow T_1$	19010	19010	$\pm 1/2$	$99.4^4H_{11/2}+0.34^4F_{7/2}+0.07^4F_{5/2}$
	525.4	5.54		$Z_1 \rightarrow T_2$	19028			
	525.2	10.8	π		19035	19038	$\pm 3/2$	$97.2^2H_{11/2}+2.29^4S_{3/2}+0.29^4F_{7/2}$
	525(sh)	4.29			19048			
	524.7	6.32	σ	$Z_1 \rightarrow T_3$	19053	19059	$\pm 1/2$	$97.9^2H_{11/2}+1.63^4S_{3/2}+0.22^4F_{7/2}$
	522.5	3.72	σ	$Z_1 \rightarrow T_4$	19133	19099	$\pm 1/2$	$99.2^2H_{11/2}+0.38^4F_{7/2}+0.22^4S_{3/2}$
	522.1	4.06	π	$Z_1 \rightarrow T_5$	19148	19103	$\pm 3/2$	$99.0^2H_{11/2}+0.48^4F_{7/2}+0.32^4S_{3/2}$
	521.4	13.3	σ	$Z_1 \rightarrow T_6$	19181	19128	$\pm 1/2$	$99.5^2H_{11/2}+2.23^4S_{3/2}+0.21^4F_{7/2}$
	520.9	12.3			19192			
$^4F_{7/2}$	490.9	0.79	σ	$Z_1 \rightarrow S_1$	20365	20369	$\pm 1/2$	$99.4^4F_{7/2}+0.43^2H_{11/2}+0.06^4F_{5/2}$
(20456)	490.7(sh)	1.77			20369			
	490.2	0.38			20394			
	489.9	0.43	π	$Z_1 \rightarrow S_2$	20407	20408	$\pm 3/2$	$98.6^4F_{7/2}+0.76^2H_{11/2}+0.40^4F_{5/2}$
	488.5	0.56			20465			
	488.3	0.76	σ	$Z_1 \rightarrow S_3$	20473	20461	$\pm 1/2$	$99.0^4F_{7/2}+0.52^2H_{11/2}+0.22^4F_{5/2}$
	486.8	1.70			20537			
	486.3	1.96	σ	$Z_1 \rightarrow S_4$	20556	20582	$\pm 1/2$	$99.5^4F_{7/2}+0.18^2H_{11/2}+0.11^4F_{5/2}$
$^4F_{5/2}$	453.3	0.68	σ	$Z_1 \rightarrow R_1$	22054	22054	$\pm 1/2$	$95.2^4F_{5/2}+4.39^4F_{3/2}+0.18^4F_{7/2}$
(22092)	453.1	0.54			22064			
	453.0	0.52	π	$Z_1 \rightarrow R_2$	22069	22062	$\pm 3/2$	$95.6^4F_{5/2}+3.74^4F_{3/2}+0.39^4F_{7/2}$
	451.8	0.24	σ	$Z_1 \rightarrow R_3$	22127	22135	$\pm 1/2$	$99.2^4F_{5/2}+0.35^4F_{3/2}+0.21^4F_{7/2}$
	451(sh)	0.20			22135			
$^4F_{3/2}$	446.6	0.28	σ	$Z_1 \rightarrow Q_1$	22385	22385	$\pm 1/2$	$94.9^4F_{3/2}+4.74^4F_{5/2}+0.10^4F_{7/2}$
(22443)	446.4	0.24			22395			
	443.8	0.13	π	$Z_1 \rightarrow Q_2$	22526	22534	$\pm 3/2$	$96.0^4F_{3/2}+3.72^4F_{5/2}+0.06^4F_{7/2}$
	443(sh)	0.10			22535			
$^2G_{9/2}$	410.0	0.13	σ	$Z_1 \rightarrow P_1$	24375	24375	$\pm 1/2$	$99.6^2G_{9/2}+0.27^2K_{15/2}+0.10^4G_{11/2}$
(24492)	409.5	0.70			24413			
	409.3	0.71	π	$Z_1 \rightarrow P_2$	24419	24427	$\pm 3/2$	$99.2^2G_{9/2}+0.55^4G_{11/2}+0.18^2K_{15/2}$
	408.6	0.53			24467			
	408.2	0.51	σ	$Z_1 \rightarrow P_3$	24491	24488	$\pm 1/2$	$99.3^2G_{9/2}+0.49^4G_{11/2}+0.10^2K_{15/2}$
	407.8	0.50	π	$Z_1 \rightarrow P_4$	24514	24534	$\pm 3/2$	$99.2^2G_{9/2}+0.47^4G_{11/2}+0.25^2K_{15/2}$
	406.7	0.67			24581			
	406.5	0.74	σ	$Z_1 \rightarrow P_5$	24590	24588	$\pm 1/2$	$99.4^2G_{9/2}+0.52^4G_{11/2}+0.04^4F_{7/2}$

[a]Multiplet manifold $^{2S+1}L_J$; number in parentheses is the calculated centroid.

[b]Wavelength in nanometers; (sh) denotes shoulder; (b) denotes broad, unresolved structure.

[c]Absorption coefficient in cm^{-1} for unpolarized spectrum; sample thickness 0.196 cm; Er concentration; approximately 4.19×10^{19} cm^{-3}; bracket indicates a grouping of peaks, in some cases partly resolved structure on an absorption band.

[d]Polarization: $\sigma(E\perp c)$, $\pi(E\|c)$; asterisk indicates incomplete polarization with either σ or π as dominant.

[e]Transition from the ground-state Stark level (Z_1) to excited-state Stark levels.

[f]Energy of Stark level in vacuum wave numbers.

[g]Calculated level based on crystal-field splitting parameters obtained from lattice-sum model and listed in Table IV; the centroids were adjusted to account for J mixing.

[h]Predicted crystal quantum symmetry label where $^1\Gamma_4+{}^1\Gamma_5\equiv\mu(\pm1/2)$ and $^2\Gamma_6\equiv\mu(\pm3/2)$, for C_3 symmetry.

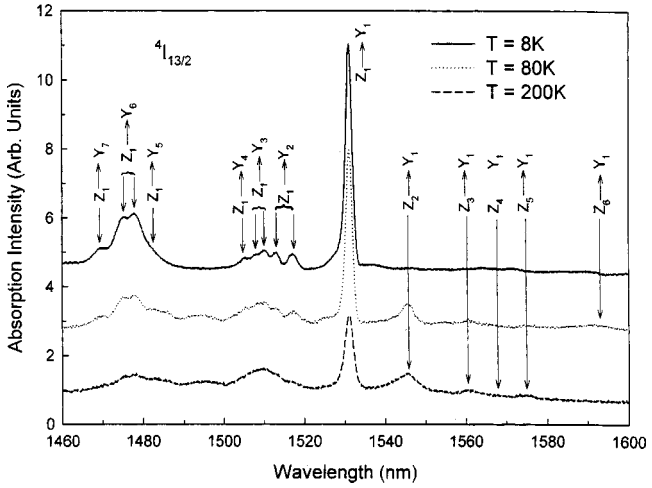

FIG. 1. Absorption spectra of the $^4I_{13/2}$ manifold, unpolarized, and obtained at 8, 80, and 200 K.

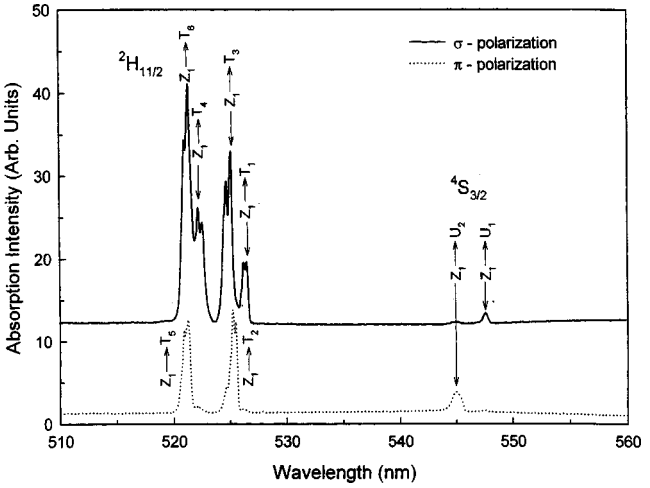

FIG. 3. Polarized absorption spectrum of the $^2H_{11/2}$ and $^4S_{3/2}$ multiplet manifolds obtained at 8 K.

associated with the absorption spectrum of the $^2H_{11/2}$ manifold (Fig. 3). Multiple Er^{3+} sites in LN have been confirmed earlier by different groups of investigators.[25,32,34,36] However, in Table I each closely spaced group of absorption peaks in a given manifold usually exhibits the same polarization behavior (see Fig. 2, for example), which suggests that the Er^{3+}-site symmetries may be similar, but have slightly different crystal-field strengths that give rise to the small energy differences that are observed between individual Stark levels in a grouping.

In Fig. 1, the intense 1531.3-nm absorption peak ($Z_1 \rightarrow Y_1$) is asymmetric with unresolved shoulders at 1532.2 and 1530 nm. The temperature-dependent peaks (hot bands) are also asymmetric with a shoulder appearing on several of these bands. Using ORIGIN software, we deconvoluted the hot-band absorption data shown in Fig. 1 and the hot-band data for $^2H_{11/2}$. The deconvoluted hot bands in Fig. 1 are identified at wavelengths 1545.8 nm (6467 cm^{-1}), 1561.7 nm (6401 cm^{-1}), 1568 nm (6376 cm^{-1}), 1576 nm (6344 cm^{-1}), and 1595 nm (6259 cm^{-1}). These hot bands represent transitions to the 6529-cm^{-1} Stark level of $^4I_{13/2}$ in Table I from Stark levels in the $^4I_{15/2}$ manifold as follows: $Z_1 = 0$, $Z_2 = 62$, $Z_3 = 128$, $Z_4 = 153$, $Z_5 = 184$, and $Z_6 = 270$, all in cm^{-1}. These levels agree with the Stark levels reported by Milori *et al.*[39] A similar set of six Stark levels for $^4I_{15/2}$ was established from the hot-band absorption spectra for the T_1 and T_2 groupings in the $^2H_{11/2}$ manifold. These six Stark levels, together with Z_7 and Z_8, are confirmed from analyses of fluorescence from the $^4S_{3/2}$ and $^4I_{13/2}$ manifolds to $^4I_{15/2}$ reported later in this study.

Different teams of investigators have suggested that the Er^{3+} ions occupy sites that have C_3 point-group symmetry.[39–44] Selection rules for electric- and magnetic-dipole transitions for Er^{3+} in these sites are as follows:[45]

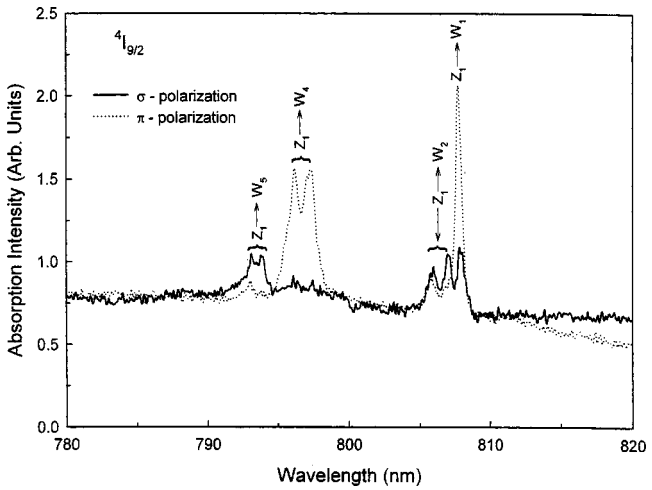

FIG. 2. Polarized absorption spectrum of the $^4I_{9/2}$ multiplet manifold obtained at 8 K.

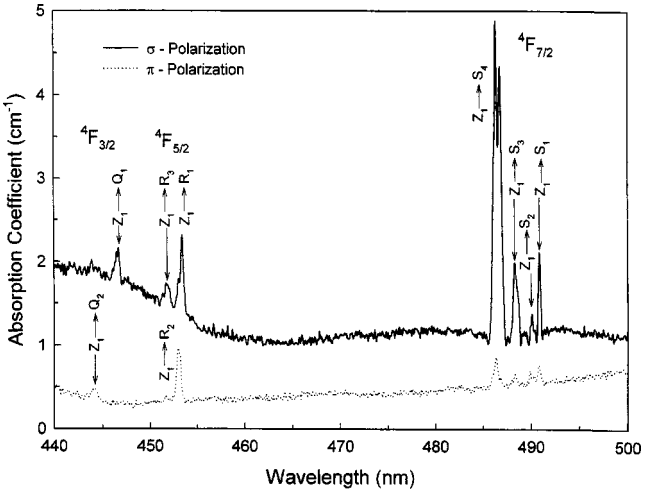

FIG. 4. Polarized absorption spectrum of the $^4F_{3/2}$, $^4F_{5/2}$, and $^4F_{7/2}$ multiplet manifolds obtained at 8 K.

		upper state		
	ED	Γ_4	Γ_5	Γ_6
lower state	Γ_4	π	σL	σR
	Γ_5	σR	π	σL
	Γ_6	σL	σR	π

where σ and π refer to polarizations when light travels perpendicular and parallel to the optic (c) axis, respectively. Here R and L refer to right and left circular polarizations when the light travels down the optic (c) axis. For M.D. (magnetic-dipole) transitions we interchange π for σ in the table, leaving R and L where they are presently placed. The labeling in the polarization table is according to Bethe.[46,47] We find it more convenient to use the labels $\mu(\pm 1/2) \equiv {}^2\Gamma_{4,5}$ and $\mu(\pm 3/2) \equiv {}^2\Gamma_6$ developed by Hellwege,[48] based on the rotational properties of the wave functions of the Stark levels.

In Table I and in Figs. 2–4 there is clear evidence for π transitions originating from the ground-state Stark level (Z_1). According to the E.D. (electric-dipole) selection rules, this means that $\mu(\pm 3/2)$ to $\mu(\pm 3/2)$ transitions are involved. Thus Z_1 is identified as a $\mu(\pm 3/2)$ crystal-quantum state and the upper Stark levels for ${}^4F_{3/2}$ and ${}^4S_{3/2}$, for example, are $\mu(\pm 3/2)$ states as well. Many of the transitions in Table I are predominantly σ polarized (in numerous cases the polarization is complete). These polarized peaks represent transitions from Z_1 to excited Stark levels whose symmetry labels are $\mu(\pm 1/2)$. Further verification of these assignments is based on circular polarization spectroscopy measurements currently underway.[49] The observed polarized spectra presented in Table I identify transitions according to crystal-quantum states and energies of Stark levels necessary for crystal-field splitting calculations, based on Er^{3+} ions in C_3 symmetry sites.

V. FLUORESCENCE SPECTRA

The fluorescence observed between 1500 and 1650 nm at 8 K, representing transitions from ${}^4I_{13/2}$ to ${}^4I_{15/2}$, is shown in Fig. 5 and listed in Table II for the unpolarized spectra obtained at 8 and 80 K. The 8-K spectra shown in Fig. 5 appear in both polarizations, although the $Y_1 \rightarrow Z_1$ transition, which is asymmetric on the high-energy side, is nearly 3 times stronger in the σ polarization. Since the Y_1 energy level is identified as a $\mu(\pm 1/2)$ Stark level in absorption (Table I), we expect a σ-polarized transition for $Y_1 \rightarrow Z_1$, representing a $\mu(\pm 1/2) \rightarrow \mu(\pm 3/2)$ transition according to E.D. selection rules for C_3 symmetry. Transitions appearing in both $\sigma\pi$ polarizations represent transitions from Y_1 $\mu(\pm 1/2)$ to $\mu(\pm 1/2)$ crystal-quantum states in the ${}^4I_{15/2}$, manifold.

The fluorescence peak at 1531.4 nm has an energy that matches the energy of the Stark level Y_1 (6529 cm^{-1}) in Table I. The energy differences based on the 8-K spectrum in Table II give a splitting for the ground-state manifold ${}^4I_{15/2}$ as follows: $Z_1=0$, $Z_2=61$, $Z_3=128$, $Z_4=155$, $Z_5=183$, $Z_6=270$, $Z_7=352$, and $Z_8=415$, all in cm^{-1}. The first six Stark levels match the levels obtained from the analysis of the hot-band absorption data and agree with the splitting reported by Milori *et al.*,[39] including Stark levels Z_7 and Z_8 (see Table III).

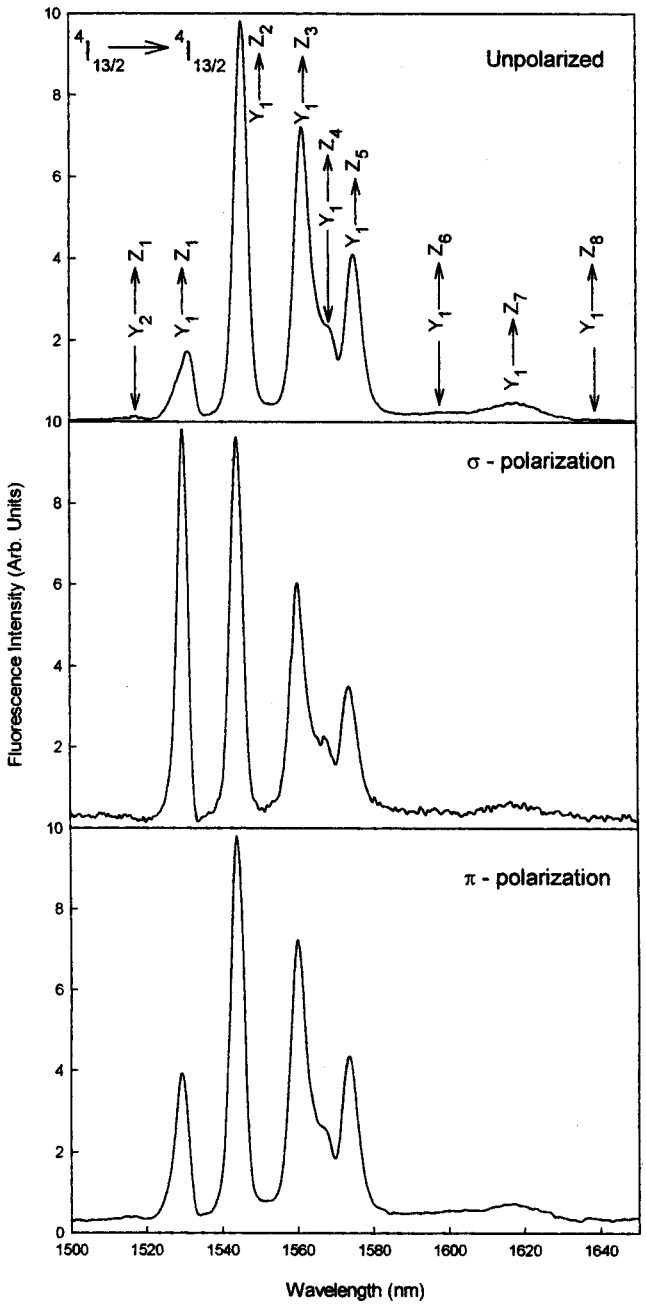

FIG. 5. Unpolarized and polarized fluorescence spectra between ${}^4I_{13/2}$ and ${}^4I_{15/2}$ multiplet manifolds obtained at 8 K.

The fluorescence spectrum between ${}^4S_{3/2}$ and ${}^4I_{15/2}$ (540–580 nm) obtained at 8 K is similar to the spectrum reported by others and does not need to be tabulated here. Transitions are observed from U_1 (Table I) to Stark levels in the ground-state manifold ${}^4I_{15/2}$ at 547.6 nm (18257 cm^{-1}), 549.5 nm (18197 cm^{-1}), 551.4 nm (18 132 cm^{-1}), 552.25 nm (18 103 cm^{-1}), 553.1 nm (18 075 cm^{-1}), 555.9 nm (17 982 cm^{-1}), 558.25 nm (17 908 cm^{-1}), and 560.5 nm (17 836 cm^{-1}). The polarization appears in both σ and π with three transitions much stronger in the σ fluorescence

TABLE II. Fluorescence from $^4I_{13/2}$ to $^4I_{15/2}$.[a]

$^{2S+1}L_J$[b]	λ (nm)[c]	I (a.u.)[d]	E (cm^{-1})[e]	Trans.[f]	ΔE (cm^{-1})[g]	λ (nm)	I (a.u.)	E (cm^{-1})	ΔE (cm^{-1})[g]
$^4I_{13/2}$	1517.5	0.88	6588	$Y_2 \rightarrow Z_1$	0	1518.0	4.75	6587	0
	1531.4	11.7	6529	$Y_1 \rightarrow Z_1$	0	1532.0	13.9	6527	0
	1545.5	66.8	6468	$Y_1 \rightarrow Z_2$	61	1546.0	26.0	6467	60
	1561.5	49.1	6401	$Y_1 \rightarrow Z_3$	128	1561.5	25.6	6402	125
	1568.5	16.0	6374	$Y_1 \rightarrow Z_4$	155	1568.5	11.7	6374	153
	1575.0	27.8	6346	$Y_1 \rightarrow Z_5$	183	1575.0	16.7	6347	180
	1598(b)	1.00	6259	$Y_1 \rightarrow Z_6$	270	1598(b)	2.62	6259	268
	1618.5	3.33	6177	$Y_1 \rightarrow Z_7$	352	1618.0	3.61	6179	348
	1635(c)	0.60	6114	$Y_1 \rightarrow Z_8$	415	1635(b)	1.22	6114	413

[a]Columns 2–6 pertain to data obtained at 8 K; columns 7–10 represent data obtained at 80 K.
[b]Emitting multiplet manifold.
[c]Wavelength in nanometers.
[d]Intensity in arbitrary units for either 8- or 80-K spectra.
[e]Energy in vacuum wave numbers.
[f]Transition from upper Stark level to Stark levels, Z_n, in $^4I_{15/2}$.
[g]Energy difference.

spectrum, which we identify as E.D. $\mu(\pm 1/2) \rightarrow \pm 3/2$ transitions. Where the intensity is comparable in both polarizations, we identify these transitions as E.D. $\mu(\pm 1/2) \rightarrow \mu(\pm 1/2)$. In summary, we obtain the splitting and symmetry labels as $Z_1=0$, $\mu(\pm 3/2)$; $Z_2=60$, $\mu(\pm 1/2)$; $Z_3=125$, $\mu(\pm 1/2)$; $Z_4=154$, $\mu(\pm 3/2)$; $Z_5=182$, $\mu(\pm 1/2)$; $Z_6=275$, $\mu(\pm 1/2)$; $Z_7=349$, $\mu(\pm 3/2)$; and $Z_8=421$, $\mu(\pm 1/2)$, all in units of cm^{-1}. Within experimental error, this splitting of the $^4I_{15/2}$ manifold agrees with the analysis of the fluorescence spectrum reported in Table II between $^4I_{13/2}$ and $^4I_{15/2}$ and also with the splitting given by Milori *et al.*[39] The fluorescence spectrum also includes additional transitions that predict part of the $^4I_{15/2}$ splitting for the Er^{3+} sites given by Witte *et al.*[25] In Table III we list the splitting of the $^4I_{15/2}$ reported by Gabrielyan *et al.*,[34] Dominiak-Dzik *et al.*,[36] Milori *et al.*,[39] and the splitting obtained from the polarized absorption and fluorescence data presented in the present study.

VI. MODELING THE CRYSTAL-FIELD SPLITTING

The energy-level structure of $Er^{3+}(4f^{11})$ is analyzed in terms of a parametrized model Hamiltonian that assumes a charge-compensated site based on the mechanism proposed by Gog *et al.*[27] having C_3 symmetry. The Hamiltonian is defined to operate within the manifold of $SLJM_J$ angular momentum states of the ground-state electronic configuration of $4f^{11}$. The total Hamiltonian consists of atomic (''free-ion'') and crystal-field terms that are spherically symmetric and crystal-field terms that are not spherically symmetric and are partitioned into the expression,

$$H_{\mathrm{cf}} = \sum_{kq} B_q^k U_q^{(k)}, \tag{1}$$

where $U_q^{(k)}$ is a unit-tensor operator of rank k and order q that is summed over all $4f$ electrons and where the B_q^k parameters

TABLE III. Stark levels of the $^4I_{15/2}$ manifold.

Level No.	E (cm^{-1})$_{expt}$ 77 K[a]	E (cm^{-1})$_{expt}$ 5 K[b]	E (cm^{-1})$_{expt}$ 4 K[c]	E (cm^{-1})$_{expt}$ 8 K[d]	E (cm^{-1})$_{expt}$ 8 K[e]	E (cm^{-1}) calc.[f]	μ calc.[f]
1	0	0	0	0	0	0	±3/2
2	63	67	63	62	61	72	±1/2
3	132	127,135	129	128	128	136	±1/2
4	156	167	152	153	155	152	±3/2
5	182	191	185	184	183	195	±1/2
6	278	—	269	270	270	301	±1/2
7	353	367	353	—	352	385	±3/2
8	414	392,443	414	—	415	412	±1/2

[a]Reference 34.
[b]Reference 36.
[c]Reference 39.
[d]This work; from hot-band absorption spectra to excited Stark levels Y_1, T_1, T_2 (Table I).
[e]This work; from $^4I_{13/2}$ 8 K fluorescence to $^4I_{15/2}$ (Table II).
[f]Predicted crystal-quantum symmetry label.

TABLE IV. Total monopole crystal-field terms for Nb, Li, and Er sites in lithium niobate.

Lat. term[a]	Nb (site)		Li (site)		Er (site)[b]		Er (B_q^k)[c]	
A_q^k	Real	Imag.	Real	Imag.	Real	Imag.	Real	Imag.
0,1	−33205	0	−21934	0				
0,2	−13980	0	−5340.8	0	−5339	0	−911	
0,3	−45522	0	7122.3	0				
3,3	16144	33214	1881.3	−10500				
0,4	−41433	0	−7442.6	0	−1386	0	−572	
3,4	21928	55742	2508.2	11183	2089	0	862	
0,5	14113	0	−6242.1	0				
3,5	1236.5	816.66	−1449.7	2137.2				
0,6	7635	0	65.806	0	66.15	0	65	
3,6	30.052	1185.7	−717.55	−346.55	−358.2	−347	−352	−341
6,6	−4706.4	4345.7	−1928.3	128.403	−193	16.28	−190	16
0,7	923.08	0	448.94	0				
3,7	−1745.3	−4252.4	−2.819	742.06				
6,7	−2608.5	2863.4	676.31	−224.9				

[a]Lattice-sum components of the crystal field in units of cm^{-1}; columns 2–6.

[b]For crystal-field splitting calculations only $k=2,4,6$ are necessary; rotation about quantization axis (c axis) reduces lattice-sum terms from 9 to 8 for C_3 symmetry.

[c]Crystal-field splitting parameters for Er^{3+} in LN used to calculate the splitting reported in Table I (column 7) and Table III (column 7).

represent the radially dependent parts of the crystal-field interaction. The operators and parameters appearing in Eq. (1) are written and defined according to conventional practice[50–54] and have been used by some of us in the past to analyze the crystal-field splitting of Nd^{3+}, Sm^{3+}, and Er^{3+} in the garnets.[55–57]

The atomic or ''free-ion part of the total Hamiltonian is of the form we used in analyzing the crystal-field splitting of the energy levels of Er^{3+} in the garnets.[55] Our initial set of atomic parameters was taken from the work of Carnall *et al.*[58] The calculated manifold centroids obtained with these parameters were adjusted by a least-squares fitting procedure to obtain the best overall agreement between calculated and observed manifolds that lead to a set of atomic parameters that we report in Table II of Ref. 59.

To establish the set of crystal-field splitting parameters defined in Eq. (1), we carried out point-charge lattice-sum calculations at the Li and Nb sites. Previous lattice-sum calculations for Er^{3+} in charge-compensated sites in host crystals of $Ca_5(PO_4)_3F$ and $Sr_5(PO_4)_3F$, where Er^{3+} resides in C_3 symmetry sites, have been helpful in setting up the lattice-sum program for Er^{3+} in C_3 sites in LN.[60–62] In considering both size and formal charge differences (Li^+, 0.68 Å ionic radius, and Er^{3+}, 0.96 Å ionic radius) Gog *et al.*[27] proposed a model where 5.9% of the lattice sites of Li^+ are occupied by Nb^{5+} ions with excess charge compensated for by Nb vacancies. The Er^{3+} ions can substitute into these sites, replacing the Nb, while the number of Nb vacancies is readjusted to establish overall charge neutrality. Figure 3 (Ref. 27) shows the hexagonal unit cell with Nb and Li sites. Abrahams and co-workers[28,29] show the complete details of the unit cell. Of special interest is Fig. 4 (Ref. 27), which shows a diagonal cut through the hexagonal unit cell of LN. The two slanted bands mark the measured coherent positions of Er atoms with respect to the $(1,\bar{1},\bar{4})$ planes, the horizontal band marks the Er position with respect to the $(0,0,\bar{6})$ planes, and the bandwidth denotes the experimental error in location. These drawings that show the position and symmetry in the unit cell of Er, Li, and Nb, and the vacancies based on the mechanism proposed by Gog *et al.*[27] provide us with the necessary information to carry out lattice-sum calculations for both the undoped and Er-doped LN crystals.

The total monopole field in terms of even and odd lattice-sum components is given as

$$A_q^k = -e^2 \sum_j q_j C_q^k(\hat{R}_j)/R_j^{n+1}, \tag{2}$$

where q_j is the effective electrostatic charge at the lattice site $(\hat{R}_j)$ and the sum is taken over all sites in the lattice.[60] The irreducible spherical tensor components of the crystal field, calculated from direct point-charge lattice sums, are defined according to conventional practice.[50,53] In Table IV we list the toal monopole crystal-field components for Nb, Li, and Er sites.

When an Er^{3+} ion is placed in the lattice, the radial part of its free-ion wave function is affected by the environment. Morrison and his associates have modeled this effect by evaluating ion-host-dependent quantities that include shielding and scaling factors introduced to account for the expansion of the radial part of the free-ion wave function.[63–66] The resulting corrections appear as a set of terms that are multiplied into the lattice-sum components to give a set of crystal-field parameters as defined in Eq. (1). In Morrison and Leavitt's calculations,[53,63–65] the one-electron crystal-field

operators are defined according to conventional practice with rank n and order m instead of k and q, respectively as given in Eq. (1). Since the even-term lattice-sum components from Eq. (2) are of primary importance for crystal-field splitting calculations, we can write the B_q^k parameters as

$$B_q^k = \rho_k A_q^k, \tag{3}$$

where $k=2,4,6$; $q=0,\pm 3,\pm 6$, with $|q| \leqslant k$. The B_q^k parameters are interrelated according to the expression

$$B_{-q}^k = (-1)^q B_q^k, \tag{4}$$

and $\rho_2=0.1706$, $\rho_4=0.4126$, and $\rho_6=0.9826$ in units of Å^n for $Er^{3+}(4f^{11})$.[64] In C_3 symmetry there are nine independent B_q^k parameters, including real and imaginary terms. By rotating the reference frame about the quantization axis[66] we can reduce the number to 8: namely, B_0^2, B_0^4, B_3^4, B_0^6, B_3^6, IB_3^6, B_6^6, and IB_6^6. The rotation is accomplished so that the imaginary A_4^3 is equal to zero.[67] Values of B_q^k are given in Table IV, and the resulting splitting is shown in Table I (column 7) and Table III (column 7). The predicted symmetry labels are also given in these tables.

VII. DISCUSSION OF RESULTS

The predicted ground-state Stark level (Z_1) (Table III, column 8) is labeled $\mu(\pm 3/2)$. According to E.D. selection rules, only $\mu(\pm 3/2) \rightarrow \mu(\pm 3/2)$ transitions are observed in the π-polarized spectrum. That π-polarized spectra are observed in the 8-K absorption spectrum (Table I), where nearly all the population resides in Z_1, not only supports the predicted symmetry for Z_1, but also predicts that the upper Stark level in each multiplet manifold, $^4S_{3/2}$ and $^4F_{3/2}$, is a $\mu(\pm 3/2)$ state as well, in agreement with the observed polarization in Figs. 2, 3, and 4. The calculated manifold splittings are also in reasonable agreement with the experimental splitting reported in Table I.

The predicted polarization and crystal-field splitting of multiplet manifolds, including $^2G_{9/2}$, $^4F_{5/2}$, $^2H_{11/2}$, $^4F_{9/2}$, and $^4I_{9/2}$, where the experimental polarization in absorption is nearly complete, are also in good agreement with the experimental data reported in Table I and the spectra shown in Figs. 2–5. In absorption, the $^4I_{11/2}$ and $^4I_{13/2}$ exhibit only partial polarization so that the predicted symmetry labels cannot be assigned with the same certainty. However, the symmetry label predictions appear to be in agreement with the dominant polarization for those transitions. The predicted symmetry label for $Y_1(^4I_{13/2})$ is a $\mu(\pm 1/2)$. Fluorescence from Y_1 and from $^4S_{3/2}U_1$ to the ground-state manifold $^4I_{15/2}$ is in agreement with the energy of the Stark levels predicted by the crystal-field splitting calculations given in Table III.

We did not attempt to fine-tune our calculations with a least-squares fitting of the Stark levels since the levels in any given multiplet grouping could not be experimentally identified further according to a particular site. In that sense, our approach follows the ''quasicenter'' concept first described by Kaminskii[68] which we used to interpret the crystal-field splitting of the energy levels of Nd^{3+} and Er^{3+} in the disordered structure of $NaBi(WO_4)_2$.[69]

The question can also be raised pertaining to more comments on the different sites. The site-selective spectroscopy reported by Gill *et al.*[32] and Witte *et al.*[25] provide important, but not enough information to cover all the multiplet manifolds of Er^{3+} necessary for us to carry out a detailed crystal-field splitting analysis to separate individual Stark levels to a particular site. The work by Rebouta *et al.*[40–42] on nonaxial sites for Er^{3+} in LN, again, is very insightful to our understanding of the complexity of the charge-compensation mechanisms that are involved. Their results together with magnetic resonance studies reported by Dischler *et al.*[43] and Milori *et al.*[39] give confirming evidence for more than one Er^{3+}-site in LN. However, it was the work of Gog *et al.*[27] that provided us with a mechanism and details for lattice-sum calculations. The present study is likely a first step in examining the charge-compensation mechanisms that are appropriate to the different Er^{3+} sites found in doped lithium niobate.

In conclusion, we present a crystal-field splitting analysis of the energy (Stark levels) of $Er^{3+}(4f^{11})$ in lithium niobate based on a lattice-sum calculation that considers the charge-compensation model as proposed by Gog *et al.*[27] The observed polarized absorption and fluorescence spectra support the assumption that the Er^{3+} site symmetries are C_3. The calculated splitting is in reasonable agreement with the groupings of the observed splitting. The calculation also predicted that the symmetry of the ground state is $\mu(\pm 3/2)$. This prediction provides a systematic and consistent interpretation to the observed polarized spectra.

[1] C. Kittel, *Introduction to Solid State Physics*, 6th ed. (Wiley, New York, 1986).
[2] J. E. Midwinter and J. Warner, J. Appl. Phys. **38**, 519 (1967).
[3] E. Krätzig and H. Kurz, J. Electrochem. Soc. **124**, 131 (1977).
[4] F. S. Chen, J. Appl. Phys. **40**, 3389 (1969).
[5] P. H. Smakula and P. C. Claspy, Trans. Soc. Min. Eng. AIME **239**, 421 (1967).
[6] G. Burns, D. F. O'Kane, and R. S. Title, Phys. Lett. **23**, 56 (1966).
[7] L. F. Johnson and A. A. Ballman, J. Appl. Phys. **40**, 297 (1969).
[8] R. C. Alferness, in *Guided Wave Optoelectronics*, edited by T. Tamir (Springer, New York, 1988), p. 145.
[9] C.-H. Huang, L. McCaughan, and D. M. Gill, J. Lightwave Technol. **12**, 803 (1994).
[10] R. Brinkmann, W. Sohler, and H. Suche, Electron. Lett. **27**, 415 (1991).
[11] P. Becker, R. Brinkmann, M. Dinand, W. Sohler, and H. Suche, Appl. Phys. Lett. **61**, 1257 (1992).
[12] *Insulating Materials for Optoelectronics*, edited by F. Agulló-López (World Scientific, Singapore, 1995).
[13] E. Desurvire, *Erbium-doped Fiber Amplifiers: Principals and Ap-*

plications (Wiley, New York, 1994).
[14] G. P. Banfi, P. K. Datta, V. Degiorgio, and D. Fortusini, Appl. Phys. Lett. **73**, 136 (1998).
[15] R. A. Becker and R. C. Williamson, Appl. Phys. Lett. **47**, 1024 (1985).
[16] A. Ashkin, G. D. Boyd, J. M. Dziedzic, R. G. Smith, A. A. Ballman, H. J. Levinstein, and K. Nassau, Appl. Phys. Lett. **9**, 72 (1996).
[17] A. Petrosyan, R. Hovsepyan, E. Kokanyan, and R. Feigelson, Proc. SPIE **4060**, 106 (2000).
[18] E. P. Kokanyan, V. G. Babajanyan, G. G. Demirkhanyan, J. B. Gruber, and S. Erdei, J. Appl. Phys. **92**, 1544 (2002).
[19] R. N. Balasanyan, V. T. Gabrielyan, E. P. Kokanyan, and I. Feldvari, Kristallografiya **35**, 1540 (1990).
[20] D. L. Veasey, J. M. Gary, J. Amin, and J. A. Aust, IEEE J. Quantum Electron. **33**, 1647 (1997).
[21] D. Scarano and I. Montrosset, IEEE J. Quantum Electron. **32**, 628 (1996).
[22] R. Brinkmann, W. Sohler, H. Suche, and C. Wersig, IEEE J. Quantum Electron. **20**, 466 (1992).
[23] W. Sohler, in Proceedings of IPR 95, paper IFCI, Dana Point, 1995.
[24] J. Y. Allain, M. Monerie, and H. Poignant, Electron. Lett. **26**, 261 (1990); **28**, 111 (1992).
[25] O. Witte, H. Stolz, and W. von der Osten, J. Phys. D **29**, 561 (1996).
[26] J. Amin, B. Dussardier, T. Schweizer, and M. Hempstead, J. Lumin. **69**, 17 (1996).
[27] Th. Gog, M. Griebenow, and G. Materlik, Phys. Lett. A **181**, 417 (1993).
[28] S. C. Abrahams, J. M. Reddy, and J. L. Bernstein, J. Phys. Chem. Solids **27**, 997 (1966).
[29] S. C. Abrahams, W. C. Hamilton, and J. M. Reddy, J. Phys. Chem. Solids **27**, 1013 (1966).
[30] G. D. Boyd, W. L. Bond, and H. L. Carter, J. Appl. Phys. **38**, 1941 (1967).
[31] M. V. Hobden and J. Warner, Phys. Lett. **22**, 243 (1966).
[32] D. M. Gill, J. C. Wright, and L. McCaughan, Appl. Phys. Lett. **64**, 2483 (1994).
[33] D. S. Moore and J. C. Wright, J. Chem. Phys. **74**, 1626 (1981).
[34] V. T. Gabrielyan, A. A. Kaminskii, and L. Li, Phys. Status Solidi A **3**, K37 (1970).
[35] V. A. Antonov and P. A. Arsen'ev, Zh. Prikl. Spektrosk. **22**, 341 (1975).
[36] G. Dominiak-Dzik, S. Golab, I. Pracka, and W. Ryba-Romanowski, Appl. Phys. A: Solids Surf. **58**, 551 (1994).
[37] E. P. Kokanyan, L. Razzari, I. Cristiani, V. Degiorgio, and John B. Gruber, Appl. Phys. Lett. **84**, 1180 (2004).
[38] V. Bermudez, M. D. Serrano, and E. Dieguez, J. Cryst. Growth **200**, 185 (1999).
[39] D. M. B. P. Milori, I. J. Moraes, A. C. Hernandes, R. R. de Souza, M. Sui Li, M. C. Terrile, and G. E. Barberis, Phys. Rev. B **51**, 3206 (1995).
[40] L. Rebouta, M. F. da Silva, J. C. Soares, D. Serrano, E. Diéguez, F. Agulló-López, and J. Tornero, Appl. Phys. Lett. **70**, 1070 (1997).
[41] L. Rebouta, P. J. M. Smulders, D. O. Boerma, F. Agulló-López, M. F. da Silva, and J. C. Soares, Phys. Rev. B **48**, 3600 (1993).
[42] L. Rebouta, M. F. da Silva, J. C. Soares, M. T. Santos, E. Dieguez, and F. Agulló-López, Opt. Mater. (Amsterdam, Neth.) **4**, 174 (1995).
[43] B. Dischler, J. R. Herrington, A. Rauber, and J. Schneider, Solid State Commun. **12**, 737 (1973).
[44] G. Burns, D. F. O'Kane, and R. S. Title, Phys. Rev. **167**, 314 (1968).
[45] R. A. Satten, Research Report No. 207, Hughes Research Laboratory, Malibu, CA, 1961.
[46] H. Bethe, Ann. Phys. (Leipzig) **3**, 133 (1929).
[47] H. Bethe, Z. Phys. **60**, 218 (1930).
[48] K. H. Hellwege, Ann. Phys. (Leipzig) **4**, 95 (1951).
[49] J. B. Gruber and D. K. Sardar (unpublished).
[50] B. R. Judd, *Operator Techniques in Atomic Spectroscopy* (McGraw-Hill, New York, 1963).
[51] H. M. Crosswhite and H. Crosswhite, J. Opt. Soc. Am. B **1**, 246 (1984).
[52] R. P. Leavitt, J. Chem. Phys. **77**, 1661 (1982).
[53] C. A. Morrison, *Angular Momentum Theory Applied to Interactions in Solids* (Springer, Berlin, 1988).
[54] M. F. Reid and F. S. Richardson, J. Phys. Chem. **88**, 3579 (1984).
[55] J. B. Gruber, J. R. Quagliano, M. F. Reid, F. S. Richardson, M. E. Hills, M. D. Seltzer, S. B. Stevens, C. A. Morrison, and T. H. Allik, Phys. Rev. B **48**, 15 561 (1993).
[56] J. B. Gruber, M. E. Hills, T. H. Allik, C. K. Jayasankar, J. R. Quagliano, and F. S. Richardson, Phys. Rev. B **41**, 7999 (1990).
[57] J. B. Gruber, B. Zandi, and M. F. Reid, Phys. Rev. B **60**, 15 643 (1999).
[58] W. T. Carnall, P. R. Fields, and K. Rajnak, J. Chem. Phys. **49**, 4412 (1968); **49**, 4424 (1968); **49**, 4443 (1968); **49**, 4447 (1968); **49**, 4450 (1968).
[59] J. B. Gruber, D. K. Sardar, B. Zandi, J. A. Hutchinson, and C. W. Trussell, J. Appl. Phys. **93**, 3137 (2003).
[60] C. A. Morrison and J. B. Gruber, Army Research Laboratory Report, ARL-TR-708, Adelphi, MD, 1994.
[61] J. B. Gruber, M. D. Seltzer, M. E. Hills, T. H. Allik, J. A. Hutchinson, C. A. Morrison, and B. H. T. Chai, Opt. Mater. **3**, 99 (1994).
[62] J. B. Gruber, C. A. Morrison, M. D. Seltzer, A. O. Wright, M. P. Nadler, T. H. Allik, J. A. Hutchinson, and B. H. T. Chai, J. Appl. Phys. **79**, 1746 (1996).
[63] R. P. Leavitt, C. A. Morrison, and D. E. Wortman, Harry Diamond Laboratories Report TR-1673, Adelphi, MD, 1975.
[64] C. A. Morrison and R. P. Leavitt, J. Chem. Phys. **71**, 2366 (1979).
[65] C. A. Morrison and R. P. Leavitt, in *Handbook of the Physics and Chemistry of Rare Earths*, edited by K. Gschneidner, Jr. and L. Eyring (North-Holland, New York, 1982), Vol. 5, p. 461.
[66] A. J. Freeman and R. E. Watson, Phys. Rev. **127**, 2058 (1962).
[67] M. E. Rose, *Elementary Theory of Angular Momentum* (Wiley, New York, 1967).
[68] A. A. Kaminskii, *Laser Crystals* (Springer, Berlin, 1981).
[69] J. B. Gruber, D. K. Sardar, C. C. Russell III, R. M. Yow, B. Zandi, and E. P. Kokanyan, J. Appl. Phys. **94**, 7128 (2003).